Computational Vibration Patterns of a Haptic Thimble for Different Placements of Embedded Piezoelectric Actuators

MSc. Robotics Thesis

Rogier O. Ketwaru

Delft University of Technology

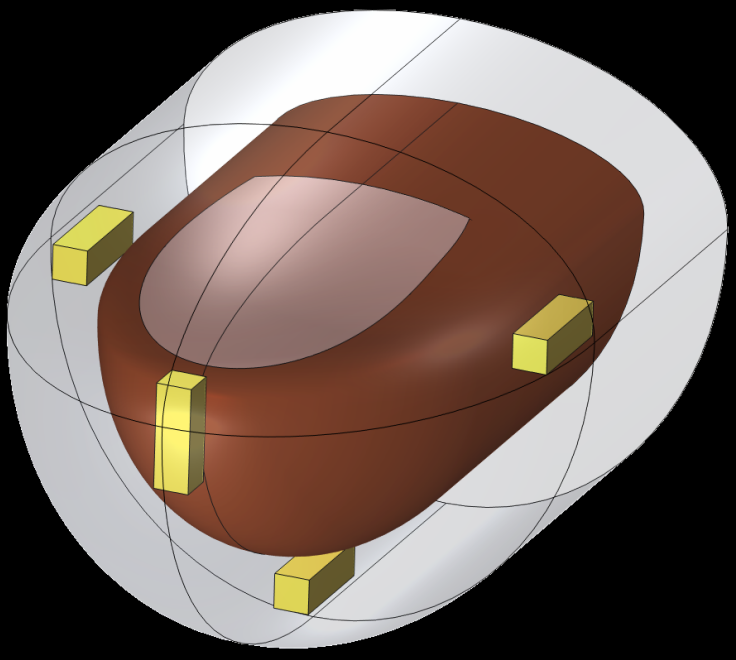

TU Delft

Computational Vibration Patterns of a Haptic Thimble for Different Placements of Embedded Piezoelectric Actuators

MSc. Robotics Thesis

by

Rogier O. Ketwaru

Student number:	4698975
Supervisors:	Dr. Y. Vardar, Dr. A. Hunt and Dr. G. Serhat
Faculty:	Cognitive Robotics
Thesis committee:	Dr. Y. Vardar, TU Delft, Chair
	Dr. A. Hunt, TU Delft, Supervisor
	Dr. G. Serhat, KU Leuven, Supervisor
	Dr.ir. S. Iskander-Rizk, TU Delft, External member

TU Delft

Acknowledgements

This journey would not have been possible, nor would I have found my destination without the support of all who helped me during this project.

First, I would like to thank Johannes Luijten from SenseGlove. Without you, I would not have been introduced to the field of wearable haptics. After the eventful internship, I asked you for graduation projects, which made me delve deeper into the world of haptics and introduced me to two of my supervisors, Yasemin Vardar and Andres Hunt.

I would also like to thank my supervisors. Yasemin Vardar and Andres Hunt, both of you were my guiding winds, especially during the exploratory phase of my thesis. Reeling me in when I was about to venture too far. Also, teaching me various lessons along the way, like improving my presentation skills, showing me how to communicate better and what it means to have your own project, while still having supervisors you can rely on. Prof. Serhat, even though you joined the team later, your help was indispensable in bringing this project to a close. With your experience with my thesis project, I could ask directed questions, which helped tremendously in furthering my understanding of the project and making me more confident in my knowledge.

Then, I would like to thank all members of HITLab I have met throughout my thesis project for the fun discussions and great feedback. To me, brainstorming with the group, while someone has a problem, was always the highlight of these meetings. Moreover, the amount of presentations I have done has made presenting so much easier and for this alone I am forever grateful.

During my master's, I have also made many new friends outside of my master's, while my friendship deepened with older ones. We shared many laughs, and it is no exaggeration when I say that you have really helped me develop as a person.

Also, a thank you to my parents, who kept me motivated throughout the years. Providing me with the support I needed and always making the atmosphere in the house lively.

Lastly, a thank you to my little brother Sjouk. You always listened when I had problems and provided ample solutions when I needed them most. I hope you are as proud of me as I am of you.

Computational Vibration Patterns of a Haptic Thimble for Different Placements of Embedded Piezoelectric Actuators

Rogier O. Ketwaru[1*], Andres Hunt[2†], Gokhan Serhat[3†], Yasemin Vardar[1†]

[1]Cognitive Robotics, Delft University of Technology, Mekelweg 5, Delft, 2628 CD, The Netherlands.

[2] Precision and Microsystems Engineering, Delft University of Technology, Mekelweg 5, Delft, 2628 CD, The Netherlands.

[3]Mecha(tro)nic Systems Dynamics Group and M-Group, KU Leuven, Oude Markt 13, Leuven, 3000, Belgium.

*Corresponding author(s)Rogier O. Ketwaru
Contributing authors: †These authors contributed equally to this work.

Abstract

This study investigates how the placement and excitation frequency of piezoelectric actuators embedded in a soft silicone haptic thimble influence displacement patterns on the human fingertip. A finite element model (HapThimb) was developed in COMSOL Multiphysics by extending the DigiTip (Serhat & Kuchenbecker, 2021) model with a 4 mm thick Ecoflex 30 layer and four tangentially acting actuators positioned on the bottom, front, and both sides of the fingertip. The model simulates both free and forced vibrations to identify resonance modes and actuator-specific deformation patterns. Free vibration analysis revealed that the addition of the thimble significantly reduced natural frequencies, with the first eigenmode shifting from 103.5 Hz (bare finger) to 45 Hz (with thimble). Moreover, the number of observed modes increased, reflecting the thimble's contribution to the complex dynamic behaviour of the system. Forced vibration analysis across the frequency range of 1–260 Hz revealed that actuator location has a strong effect on both the amplitude and spatial distribution of displacements. The bottom actuator yielded the highest local response (53.8 µm at 185 Hz), while the front actuator produced weaker, and localised responses. The side actuators, activated in-phase, resulted in the broadest and most versatile vibrational patterns, exciting multiple finger regions with peaks up to 41.4 µm. These findings highlight the importance of actuator placement in achieving desired tactile effects. The results inform design strategies for wearable haptic devices by identifying configurations that maximise vibrational efficiency and spatial selectivity.

Keywords: Human fingertip, Finite element methods, Piezoelectric actuator, Modal analysis

1 Introduction

Tactile information is transmitted from the skin to the central nervous system through mechanoreceptors embedded in the glabrous (non-hairy)

skin of the human hand (Johnson, Yoshioka, & Vega-Bermudez, 2000). These mechanoreceptors respond to diverse stimuli, contributing to sensations such as slip detection (Srinivasan, Whitehouse, & LaMotte, 1990), form perception (Johnson & Hsiao, 1992), and the detection of both low- and high-frequency vibrations (Brisben, Hsiao, & Johnson, 1999). Accurate and effective stimulation of these receptors has significant applications in fields such as teleoperation, virtual reality (VR), and augmented reality (AR), where high-fidelity tactile feedback can greatly enhance immersion and interaction (Kim, Jeon, & Kim, 2017).

One of the key challenges in developing tactile interfaces for these applications is wearability, which directly impacts comfort, usability, and user immersion (Pacchierotti et al., 2017). A critical component of wearable haptic systems is the actuator. Among available options, piezoelectric actuators have emerged as particularly promising due to their compact form factor, rapid dynamic response, and high displacement resolution (Huang et al., 2022). These actuators function by expanding and contracting in response to an applied voltage.

However, the effectiveness of piezoelectric stimulation is not determined solely by actuator performance. Instead, it is mediated by the mechanical coupling between the actuator, the wearable structure (e.g., a thimble), and the human fingertip. Parameters such as actuator placement and system dynamics play a critical role in shaping the spatial and temporal characteristics of the resulting tactile signal (Blanco-Diaz et al., 2024). Despite their importance, these factors have received limited systematic investigation in the context of wearable fingertip devices. A deeper understanding of how mechanical configurations affect tactile outcomes could enable more efficient stimulation strategies, possibly reducing the number of actuators needed to produce a diverse set of perceptual cues.

To address the gap, this study has utilized finite element modelling (FEM) to simulate the vibrational behaviour of a haptic thimble fingertip system. FEM allows for high-fidelity predictions of stress, strain, and displacement fields under varying structural and excitation conditions (Wu, Krajnak, Welcome, & Dong, 2009), making it an effective tool for pre-prototyping and design optimization in wearable haptics.

The fingertip model developed in this study has been built on the DigiTip framework (Serhat & Kuchenbecker, 2021), and incorporates multiple tissue layers, including the stratum corneum, bulk tissue, nail bed, and fingernail, to accurately capture the spatial variability in stiffness and material behaviour. This layered architecture has been critical for resolving local resonances and understanding how actuator energy propagates through the finger-thimble system.

A central component of the analysis was the use of free vibration analysis to identify natural frequencies and mode shapes of the coupled system. These eigenmodes represent the deformation patterns most likely to be excited by external actuation and have served as a basis for interpreting the system's resonant behaviour. Understanding these vibrational characteristics has allowed for targeted analysis of how actuator configuration affects both amplitude and spatial distribution of deformation across the fingertip.

This study aims to answer the following central research questions:

How do the placement and excitation frequency of piezoelectric actuators embedded in a haptic thimble worn on the finger affect displacement patterns on the fingertip?

With the following supporting subquestions:

- *What is the effect of the haptic thimble on the free vibration modes of the finger-thimble system?*
- *How does fingertip deformation differ between the site of excitation and other regions of the finger between actuator placements during forced vibration?*

By answering these questions, the study seeks to inform design principles for more efficient and perceptually effective wearable haptic thimbles.

2 Material and Methods

2.1 The Finger

The model consists of seven distinct layers: the silicone thimble, stratum corneum, bulk tissue, hypodermis, nail plate, nail bed, and bone. As this model extends the DigiTip (Serhat & Kuchenbecker, 2021) model by incorporating a haptic thimble, it is hereafter referred to as HapThimb. Except for the simplification of replacing separate

dermis and epidermis layers with a single bulk tissue layer, the geometry and material properties of the finger are largely identical to those used in the DigiTip model by (Serhat & Kuchenbecker, 2021).

The hypodermis layer is modelled using quarter ellipsoids for the fingertip's anterior region and eccentric cone segments for the posterior region. The nail plate and nail bed are also modelled with eccentric cones, which may differ slightly from the original approach in the DigiTip model Serhat and Kuchenbecker (2021). This hybrid design ensures a smooth geometric transition and more realistic anatomical curvature. The same approach for modelling the hypodermis layer has been applied to the subsequent soft tissue layers.

Material properties for each anatomical layer are provided in Table 1. The distal phalanx (the fingertip bone) is assumed to be rigid due to its significantly higher elastic modulus compared to soft tissues (Turner, Rho, Takano, Tsui, & Pharr, 1999), and a fixed constraint is applied to all the nodes bordering the surface of the bone domain. All other tissues are modelled as linearly elastic, and the proximal surface, connecting the fingertip to the rest of the finger, is left free, representing a natural joint boundary.

2.2 The Thimble

The thimble is modelled similarly to the other skin layers but includes four embedded piezoelectric actuators. These are located halfway between the outer silicone layer and the outer finger skin, with placements categorised as follows (see Figure 1):

- Bottom actuator: Located centrally beneath the fingertip, aligned with the transition zone between the lower ellipsoid and conical segment of the thimble.
- Side actuators: Placed symmetrically on the right and left sides of the nail, also on a transition point between the ellipsoids and cone segments. These actuators are activated together, in phase, to prevent asymmetrical vibrations.
- Front actuator: Positioned at the anterior face of the fingertip, where the middle of this actuator is 1 mm below the middle of the side actuators to accommodate the geometry of the thimble.

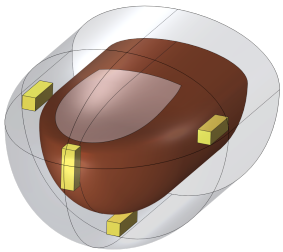

Fig. 1: HapThimb model to show the placements of the four actuators (in yellow)

All actuators operate by expanding and contracting along their longitudinal axis. A displacement of ±2 µm is applied to each end, resulting in a total stroke of 4 µm. Notably, this direction of actuation is tangential to the skin surface, contrasting with the more common normal direction used in prior literature for haptic stimulation devices and FEM studies(Leroy, Hinchet, and Shea (2020),Gertler, Serhat, and Kuchenbecker (2023)).

Instead of pushing into the skin, these actuators stretch the thimble tangentially to generate tactile feedback. The main reason for this choice was to make the design as compact as possible. Placing the actuators in an orientation where the direction of actuation would be normal to the skin surface would drastically increase the thickness of the thimble, either locally or over the whole thimble. This increase could hurt the efficiency of vibration transmissibility. The other tangential orientation, perpendicular to the chosen one, could cause local curvatures in the thimble, also lessening the vibration transmission. Actuators oriented in the direction of the finger, the direction used in this study, could produce more global effects on the thimble and thus on the finger.

The thimble is composed of Ecoflex 30, a silicone material widely used in soft robotics and haptic interfaces due to its skin-like compliance and high elasticity (Case, White, & Kramer, 2015). It is modelled as linearly elastic, consistent with the finger layers. Table 2 summarises the material properties and dimensions of the thimble and actuators.

The actuator operation is approximated in COMSOL using prescribed displacement nodes.

Table 1: The values for density, Poisson's ratio and elastic modulus for the five layers of the finger part of HapThimb

	Stratum Corneum	Bulk Tissue	Hypodermis	Nail Bed	Fingernail
Elastic modulus (MPa)	1.000[1]	0.010[2]	0.034[1]	1.000[1]	170.0[1]
Poisson's ratio	0.30[1]	0.48[2]	0.48[1]	0.30[1]	0.30[1]
Density (g/cm^3)	1.100[3]	1.000[2]	0.920[4]	1.100[1]	1.300[5]

[1] From (Somer, Perić, de Souza Neto, & Dettmer, 2015)
[2] From (Nam & Kuchenbecker, 2021)
[3] From (Marks, Barton, & Edwards, 2012)
[4] From (Störchle et al., 2018)
[5] From (Mckittrick et al., 2012)

Table 2: The values for density, Poisson's ratio, elastic modulus and dimensions of the thimble part of HapThimb

Variable	Value
Thimble thickness (mm)	4.000
EcoFlex 30 elastic modulus (MPa)	0.027[1]
EcoFlex 30 Poisson's ratio	0.4287[1]
EcoFlex 30 density (g/cm^3)	1.000[1]
Actuator dimensions (mm)	1.650x1.650x5.000[2]
Actuator elastic modulus (MPa)	49,000[3]
Actuator Poisson's ratio	0.32[3]
Actuator density (g/cm^3)	7.600[3]

[1]From (Mathur, Mak, Naghibi, & Abayazid, 2021)

[2]From Aliexpress

[3]Assumed to be equivalent to PZT-2 from https://www.efunda.com/materials/piezo/general_info/gen_info_index.cfm

Each actuator's ends are given a static displacement of ±1 µm and a harmonic perturbation node. This allows for time-varying sinusoidal oscillation, enabling expansion and contraction throughout a frequency sweep between 1 and 260 Hz with increments of 1 Hz where 260 Hz is around the maximum sensitivity frequency of the human hand (Gescheider, Bolanowski, Pope, & Verrillo, 2002).

All parameters in the HapThimb model are fully parameterised, making it adaptable for simulations involving other finger sizes, thimble designs, or actuator configurations. Exact dimensions used in this study can be found in Appendix A.

3 Validation

3.1 Mesh Convergence Study

To validate the model, a mesh convergence study was conducted. Four progressively finer meshes were generated using COMSOL Multiphysics' automatic meshing presets: *extra coarse*, *coarser*, *coarse*, and *normal*. These meshes consisted of 10,775, 22,937, 46,851, and 91,015 free tetrahedral elements, respectively, representing an approximate doubling of element count at each refinement step.

Figure 2 illustrates the convergence behaviour across the first 12 eigenmodes for each mesh. The differences in natural frequencies between successive refinements were found to be minimal beyond the *coarse* mesh, indicating asymptotic convergence. Based on this analysis, the *normal* mesh preset (91,015 elements, 16,005 nodes) was selected for all subsequent simulations (see Figure 3) to ensure both accuracy and computational efficiency. The difference observed between the *normal* and *coarse* mesh was less than 0.2%.

The total volume of the meshed domain is 11,350.0 mm^3, yielding an average element density of approximately 8.019 elements/mm^3, or equivalently, 0.125 mm^3 per element. Due to the use of displacement fields in COMSOL, the number of degrees of freedom for HapThimb using this preset is 373,020.

3.2 Comparison DigiTip

To further validate the model, a direct comparison was performed between the free vibration eigenmodes of HapThimb and those reported in the DigiTip model (Serhat & Kuchenbecker, 2021). Since the geometry and dimensional parameters of

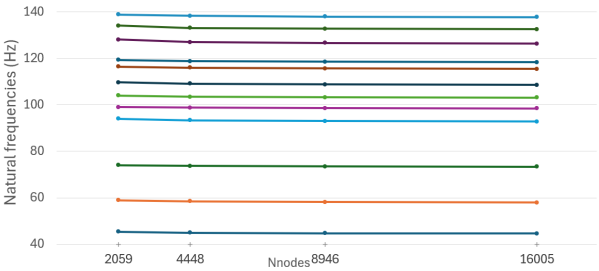

Fig. 2: Mesh convergence graph using the extra coarse, coarser, coarse and normal COMSOL Multiphysics presets for the first 12 eigenmodes of HapThimb

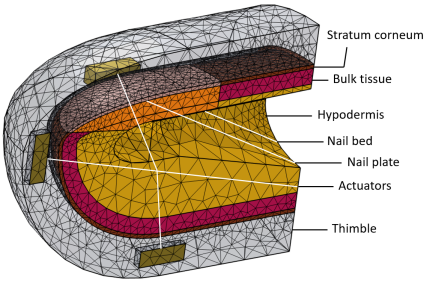

Fig. 3: Section view of the HapThimb model normal preset mesh with all shown layers annotated.

the finger segment are functionally identical, a free vibration analysis was conducted on the bare finger version of the model to isolate the mechanical behaviour of the fingertip.

Firstly, the mathematical basis of free vibration analysis will be explained. During free vibration, no external forces affect the system, meaning the equation of motion can be written as:

$$\mathbf{M}\ddot{\mathbf{u}}(t) + \mathbf{K}\mathbf{u}(t) = \mathbf{0} \tag{1}$$

K and M are global stiffness and mass matrices, respectively, whose size is governed by the number of degrees of freedom in the mesh (504,885). A complex harmonic displacement solution is assumed with $u = U_n e^{i\omega_n t}$ with $i = \sqrt{-1}$ resulting in the following eigenvalue equation:

$$(\mathbf{K} - \omega_n^2 \mathbf{M})U_n = \mathbf{0} \tag{2}$$

Here ω_n are the natural frequencies in radians per second obtained by solving the determinant of $(K - \omega_n^2 M) = 0$. U_n are the nodal mode shape vectors that correspond to ω_n(Harris & Piersol, 2002).

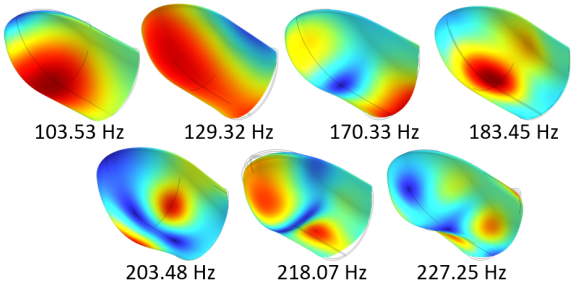

Fig. 4: The first seven free vibration modal shapes using only the finger part of HapThimb, where the higher and lower relative displacements are shown using warmer(red) and colder(blue) colours, respectively. Natural frequencies of every eigenmode are shown underneath their respective shape.

As shown in Figure 4, the modal shapes produced by the bare finger model closely resemble those reported for DigiTip. The first mode in both models exhibits torsional deformation around the distal phalanx. Mode two displays a rotation around the lateral axis, consistent across both models. Mode three similarly involves lateral motion in the distal region of the finger with some torsional deformation near the attachment boundary, slightly more apparent in the bare finger model compared to DigiTip.

From mode four onward, minor differences become more apparent. In the model, the fourth mode features contraction and expansion predominantly near the distal part of the finger compared to DigiTip. In mode five, DigiTip presents out-of-phase surface-normal motions near the lower-left and -right regions of the fingerpad; these motions are less pronounced in the bare finger model and appear shifted more distally.

Mode six in both models displays out-of-phase lateral movement. Mode seven in the bare finger model captures a similar pattern to DigiTip, with alternating contraction in the distal-left and proximal-right regions and outward expansion on the opposing sides, albeit with a somewhat reduced amplitude.

One notable difference is the natural frequency spectrum. The bare finger model exhibits lower natural frequencies across corresponding modes compared to DigiTip. This discrepancy is likely

Table 3: The found first seven eigenfrequencies of the bare finger HapThimb model of the free vibration analysis compared to the first seven free vibration frequencies of DigiTip(Serhat & Kuchenbecker, 2021).

Mode	Bare finger (Hz)	DigiTip (Hz)
1	103.53	122.4
2	129.32	163.7
3	170.33	194.0
4	183.45	225.0
5	203.48	231.8
6	218.07	254.1
7	227.25	256.8

due to structural modelling differences: DigiTip treats the epidermis and dermis as separate layers, while HapThimb uses a bulk material representation. Additionally, DigiTip employs hexahedral meshing, whereas the HapThimb model uses tetrahedral elements, which may affect numerical stiffness and frequency resolution.

Despite minor variations, the HapThimb model replicates the key dynamic features of the DigiTip eigenmodes with high fidelity. This close agreement confirms that the HapThimb fingertip model produces valid vibrational behaviour and supports its use in further free and forced vibration analyses.

4 Results

4.1 Free Vibration Analysis

Table 4: The found first seven eigenfrequencies of the bare finger model of the free vibration analysis compared to the first seven free vibration frequencies of HapThimb with the thimble.

Mode	Bare finger (Hz)	HapThimb (Hz)
1	103.53	44.584
2	129.32	57.945
3	170.33	73.362
4	183.45	92.765
5	203.48	98.492
6	218.07	103.07
7	227.25	108.61

Table 4 presents a comparison between the first seven eigenfrequencies of the bare finger model and the HapThimb model equipped with the thimble. The results demonstrate that the addition of the soft silicone thimble substantially reduces the system's natural frequencies. For example, the first mode decreases from 103.53 Hz in the bare finger model to 44.584 Hz in HapThimb. In addition to lower natural frequencies, the presence of the thimble also increases the modal density within a given frequency band. For the bare finger, the first seven modes are distributed over a bandwidth of 123.72 Hz (from 103.53 Hz to 227.25 Hz), whereas the same number of modes in the HapThimb model are concentrated within a narrower bandwidth of 64.026 Hz (from 44.584 Hz to 108.61 Hz).

4.2 Forced Vibration Analysis

The results of each forced vibration scenario are presented in two parts:

In the first part, the average displacement across the outer layer of the fingertip (the stratum corneum) is presented while the actuator(s) sweep through a frequency range of 1–260 Hz. This analysis provides an overview of how excitation frequency influences overall displacement magnitude. Peaks in these displacement curves that align with the system's free vibration eigenfrequencies are highlighted, as they indicate the potential presence of resonances. These resonance points are of particular interest for haptic applications, where amplified displacements can enhance tactile feedback.

The second part focuses on the localised behaviour of the finger skin near each actuator. Four probe points were positioned at the boundary between the thimble and the fingertip, each placed perpendicular to one of the actuator sites (bottom, front, and both sides). These probes monitor site-specific displacements across the entire excitation spectrum, allowing for detailed examination of how and where resonant modes manifest in the structure. This local perspective complements the global average analysis and provides insight into which actuator placements are most effective at exciting desired displacement patterns.

During forced vibration analysis, if a harmonic displacement affects the system, the equations of motion become:

$$\mathbf{M}_{ff}\ddot{\mathbf{u}}_f(t)+\mathbf{M}_{fp}\ddot{\mathbf{u}}_p(t)+\mathbf{K}_{ff}\mathbf{u}_f(t)+\mathbf{K}_{fp}\mathbf{u}_p(t)=\mathbf{0} \quad (3)$$

Where u_p is the prescribed displacement vector and u_f the free displacement computed by COMSOL. Since the displacements are purely harmonic with $u_p(t) = \hat{u}_p e^{i\omega t}$ and $\ddot{u}_p(t) = -\omega^2 \hat{u}_p e^{i\omega t}$, then the equation in the frequency domain becomes:

$$(-\omega^2\mathbf{M} + \mathbf{K})u = 0 \quad (4)$$

Here, these $\mathbf{M}$ and $\mathbf{K}$ matrices are both the same as in the free vibration scenario and the simulation will solve for u.

This section will be divided in the same manner as the actuator categories: bottom, front and side actuators.

4.2.1 Bottom Actuator

4.2.1.1 Average Displacement Analysis

Figure 5 presents the average displacement response of the stratum corneum during forced vibration of the bottom actuator, with excitation frequencies sweeping from 1 to 260 Hz. The grey dashed lines indicate the eigenfrequencies obtained from the free vibration analysis. Where these lines intersect displacement peaks, potential resonance behaviour is suggested.

In the low-frequency range (below 100 Hz), three peaks are observed. The first, around 45 Hz, is small but aligns with the first eigenfrequency. A second, more prominent peak appears at approximately 94 Hz. Between these, a moderate peak arises that does not correspond to any identified free vibration mode, suggesting the possibility of a localised resonance.

Larger peaks begin to appear from 175 Hz that confidently break the threshold of 10 µm, most notably the peaks at 175 Hz (12.7 µm), 185 Hz (22.6 µm), 252 Hz (18.9 µm) and 257 (25.4 µm). The resonance density also increases quite dramatically between 200 and 250 Hz.

Between 100 Hz and 170 Hz, few notable peaks are present, and average displacement amplitudes remain low, typically within the 1–3 µm range. This frequency band appears less responsive to actuator excitation.

Above 170 Hz, several larger displacement peaks emerge. Notable examples include those at 175 Hz (∼12.7 µm), 185 Hz (∼22.6 µm), 252 Hz (∼18.9 µm) and 257 Hz (∼25.4 µm). These values significantly exceed the 10 µm threshold, indicating strong system responses. Additionally, the density of resonant peaks increases substantially in the 200–250 Hz range. This suggests that multiple higher-order modes are being activated by the bottom actuator in this frequency band.

4.2.1.2 Local Response Analysis

Figure 6 shows the average displacement measured at the four probe locations, each situated near an actuator site (bottom, front, and sides). Overall, the probe near the bottom actuator consistently recorded the highest displacement amplitudes, particularly in the low-frequency range and across most resonance peaks, with the highest peak at 53.8 µm at 185 Hz.

While the bottom site generally dominates the displacement response between 120 and 210 Hz, there are notable exceptions. At 103 Hz, for instance, the front probe records a slightly higher amplitude than the bottom probe, by a few microns, suggesting spatial variability in mode shape expression. Similarly, at 175 Hz (14.6 µm), the side probes record displacement amplitudes comparable to the bottom probe.

Above 210 Hz, where the density of resonances increases, the bottom probe continues to exhibit the highest displacements in most cases. However, certain modes show localised amplification at other sites: for example, 4.10 µm at the side probe at 209 Hz, and 6.46 µm at the front probe at 217 Hz. The most significant deviation occurs at 257 Hz, where the front probe records a large peak of 36.1 µm, exceeding the bottom probe's response and indicating a high-frequency mode with dominant deformation at the front of the fingertip.

4.2.2 Front Actuator

4.2.2.1 Average Displacement Analysis

Figure 7 presents the average displacement of the stratum corneum during excitation by the front actuator over the frequency range of 1–260 Hz. Compared to the bottom and side actuator scenarios, the response in this configuration is notably lower in magnitude. Most peaks remain below 10 µm, with the majority ranging between 2–5 µm.

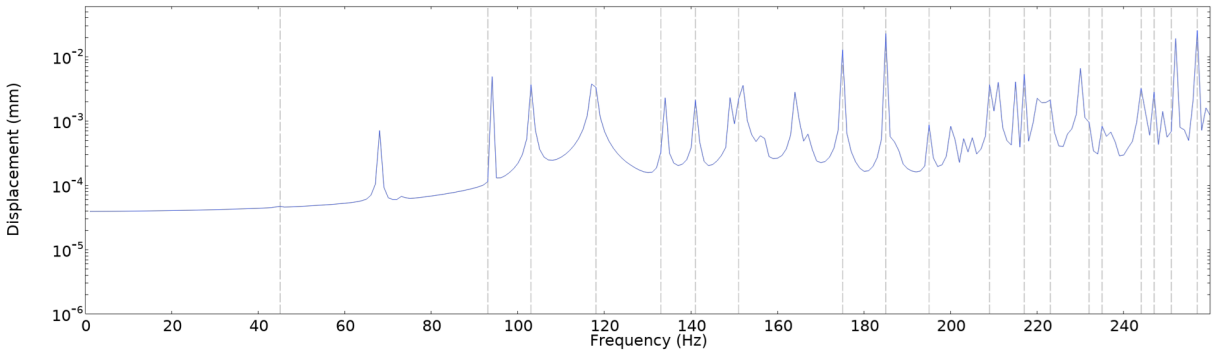

Fig. 5: Graph containing average displacement of the stratum corneum while the bottom actuator is excited. The dashed lines are the free vibration modal frequencies that intersect the peak frequencies.

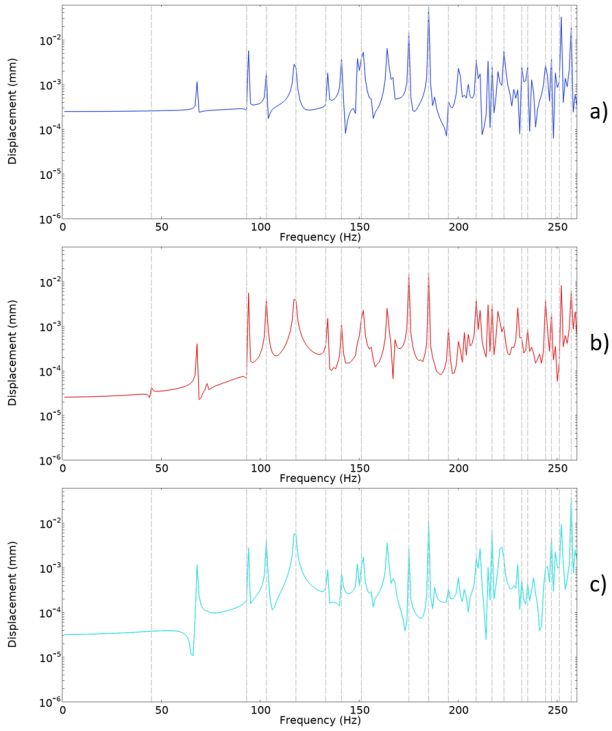

Fig. 6: Graphs containing the average displacements at four probes on the finger perpendicular to the sites of actuation. Plots a, b and c display the displacements recorded by the bottom, side and front probes, respectively. In these graphs, the bottom actuator is excited.

The highest displacement peak occurs at 252 Hz, reaching 16.2 µm, while the second-largest appears at 228 Hz, with a value of 10.7 µm. Aside from these two, no other peaks exceed the 10 µm threshold, indicating a generally weaker average system response under front actuator excitation.

4.2.2.2 Local Response Analysis

Local probe data in Figure 8 further support the observation that the front actuator exhibits limited effectiveness in exciting large fingertip displacements. Up to 133 Hz, the bottom and side probes register slightly higher responses than the front probe.

Beyond 140 Hz, this trend becomes more pronounced. The bottom probe dominates the local response spectrum across several resonant peaks. Notably, the peaks at 185 Hz (15.0 µm), 226 Hz (10.8 µm) and 228 Hz (14.1 µm) show displacements between two and three times higher than in the front probe.

4.2.3 Side Actuators

4.2.3.1 Average Displacement Analysis

Figure 9 shows the average displacement response of the stratum corneum when the side actuators are simultaneously excited across the 1–260 Hz frequency range. Several small displacement peaks are observed below 100 Hz, unique to this scenario and absent in the bottom and front actuator cases.

The most notable are the peaks at 118 Hz (17.7 µm), 175 Hz (15.0 µm), 204 Hz (13.6 µm), 213 Hz (15.8 µm), 245 Hz (41.4 µm) and 254 Hz (17.1 µm). The highest peak is at 245 Hz with an average displacement of 41.4 µm. The elevated response amplitudes across a broad frequency band may be attributed to constructive interference from dual-actuator excitation.

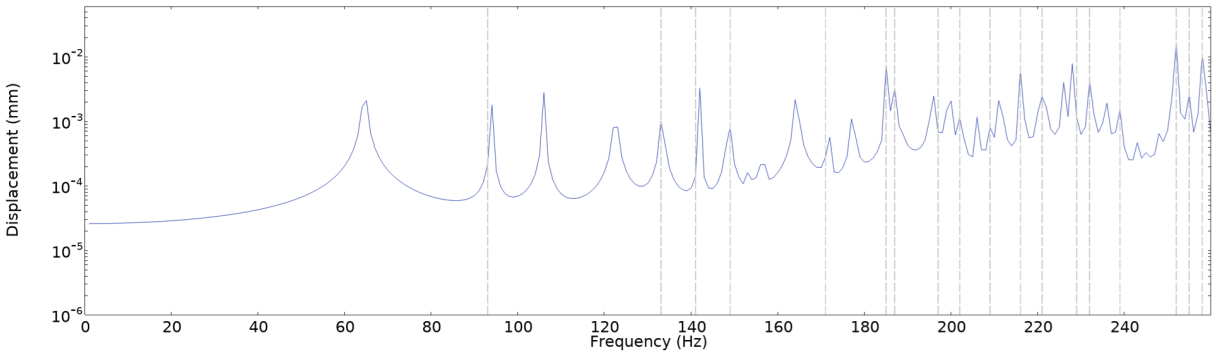

Fig. 7: Graph containing average displacement of the stratum corneum while the front actuator is excited. The dashed lines are the free vibration modal frequencies that intersect the peak frequencies.

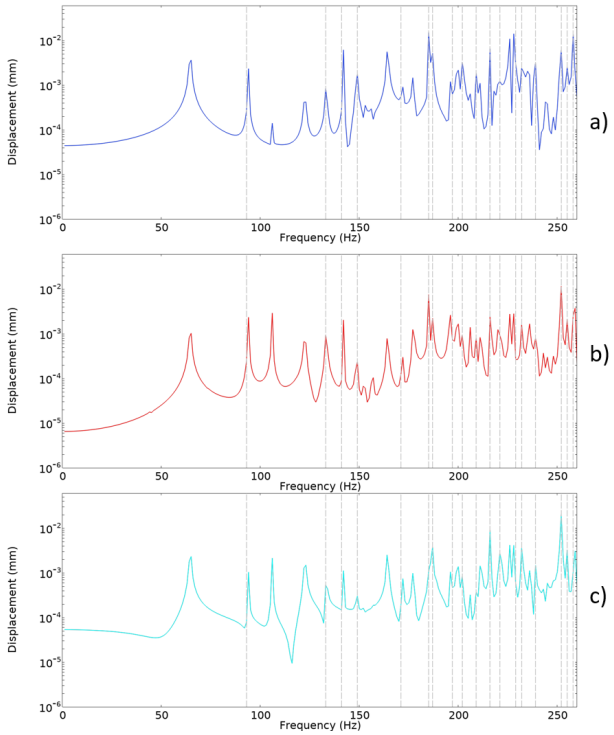

Fig. 8: Graphs containing the average displacements at four probes on the finger perpendicular to the sites of actuation. Plots a, b and c display the displacements recorded by the bottom, side and front probes, respectively. In these graphs, the front actuator is excited.

4.2.3.2 Local Response Analysis

The local probe data in Figure 10 provides additional insight into the spatial distribution of the potential resonances. Initially, below 100 Hz, the side probes register the highest displacement values, consistent with direct excitation. However, beyond this point, significant responses are observed across all probe locations, indicating broad modal participation.

At 118 Hz, displacements at the front (19.7 µm) and side (18.8 µm) probes are nearly identical. Between 142–157 Hz, the bottom probe exhibits dominant activity, peaking at 150 Hz with 20.9 µm. Similarly, the resonance at 175 Hz is shared between the bottom (22.8 µm) and front (17.9 µm) probes.

The resonance at 204 Hz is primarily composed of contributions from the bottom (32.5 µm) and front (15.0 µm) probes, while at 213 Hz, a localized response is observed exclusively at the side probe (15.7 µm). At 238 Hz, the peak response arises from the bottom (20.0 µm) and side (14.8 µm) probes, suggesting mixed-mode participation.

The peak at 245 Hz shows the most significant system-wide deformation, with displacements of 44.4 µm (bottom), 42.5 µm (side), and 31.3 µm (front), indicating a global resonance involving all actuator regions. Finally, at 254 Hz, the side probe again records a localised peak of 17.9 µm, supporting the presence of another high-frequency local resonance.

4.3 Limitations

While the FEM simulations conducted using COMSOL Multiphysics provide valuable insights into the vibrational behavior of the HapThimb system, several limitations should be acknowledged.

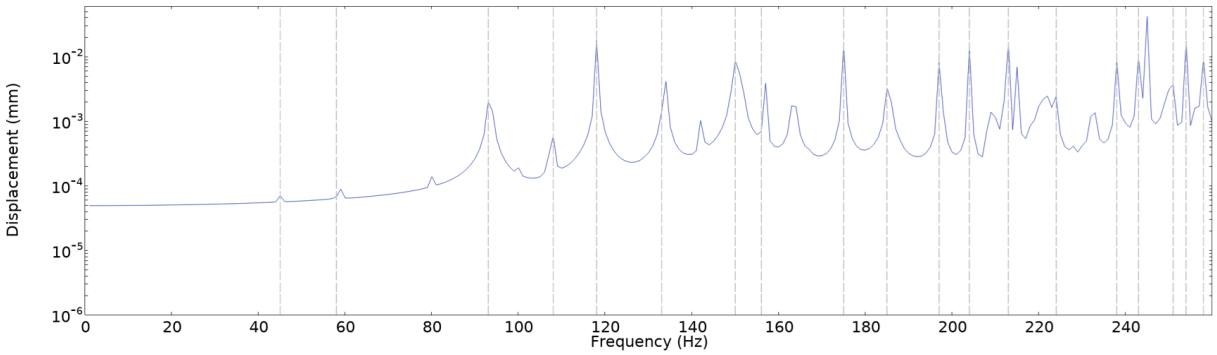

Fig. 9: Graph containing average displacement of the stratum corneum while the side actuators are excited. The dashed lines are the free vibration modal frequencies that intersect the peak frequencies.

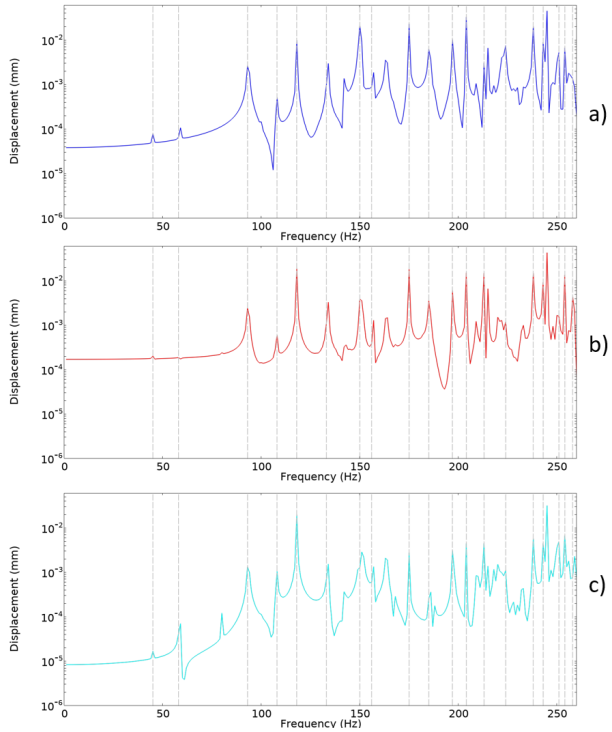

Fig. 10: Graphs containing the average displacements at four probes on the finger perpendicular to the sites of actuation. Plots a, b and c display the displacements recorded by the bottom, side and front probes, respectively. In these graphs, the side actuators are excited.

First, the forced vibration studies employed harmonic displacement inputs rather than harmonic forces, like in DigiTip (Serhat & Kuchenbecker, 2024). This modelling choice implies that displacements were prescribed directly, without accounting for the force required to achieve them, particularly relevant at higher frequencies where inertial and stiffness effects become more pronounced. The reason for this choice was that the actuator models in HapThimb are based on existing piezoelectric actuators(see table 2). Maximum displacements were approximated based on similarly sized actuators from Thorlabs. For improved accuracy, future work could involve direct experimental characterisation of these actuators to develop realistic harmonic force inputs.

Second, the current model is formulated under linear elastic assumptions, meaning it is valid primarily for small-strain, small-displacement regimes. At higher excitation levels, nonlinear material behaviour or geometric effects may become significant. This may help explain the anomalously large peak observed at 68 Hz in Figure 5, which could result from numerical amplification outside the linear regime. Incorporating nonlinear material models and amplitude-dependent damping could address this in future studies.

Third, the simulations assume steady-state harmonic behaviour, excluding any transient dynamics. However, transient responses can play a crucial role in tactile perception, particularly during contact onset and release (Shao, Hayward, & Visell, 2016). While steady-state analysis reveals resonant characteristics, it may not fully capture temporal effects relevant to perception and usability.

Additionally, the geometric model of the finger is based on average male index finger dimensions, with material properties derived from literature. In reality, anatomical variations in fingertip size,

shape, and tissue stiffness due to age, gender, or individual differences can significantly alter vibration response (Abdouni et al., 2017). These variations are not accounted for in the current study, limiting generalizability.

5 Discussion

When compared to the HapThimb model without the thimble (Table 4), the introduction of the silicone layer results in a pronounced decrease in natural frequencies. The first eigenfrequency without the thimble is 103.53 Hz, compared to 45 Hz in the whole model. This reduction can be explained by the classic mass–spring relationship:

$$\omega_n = \sqrt{\frac{k}{m}} \tag{5}$$

Where k is the stiffness of the damper and m is the mass. The thimble introduces additional mass to the system without a proportionate increase in stiffness, thereby reducing the natural frequencies.

Additionally, the number of modes observed between 1 and 260 Hz exceeds 80 in the full model, compared to only nine modes in the finger-only configuration. Parametric testing revealed that thicker thimble layers further increase the number of modal resonances, while thinner layers reduce it. This behaviour likely results from the high compliance of the thimble material, which allows localised resonant modes to emerge throughout the structure.

As presented in subsection 4.2.1, the bottom probe exhibits the largest displacement amplitudes across the full excitation range. This is attributed to the bottom actuator's location away from the stiff nail plate and nail bed, which permits more efficient vibratory energy transfer. The peak response of 53.8 µm at 185 Hz is the highest displacement recorded by a point probe in this study, confirming strong actuator structure coupling. The second-largest peak, recorded at the front probe, is likely linked to the actuator's longitudinal excitation, which may induce rotational deformation around the lateral axis, explaining the upward displacement observed at the front probe.

As discussed in subsection 4.2.2, the front actuator produces relatively subdued responses. Its placement directly in front of the nail plate introduces significant mechanical impedance, which limits displacement transmission. At lower frequencies, the bottom and side probes exhibit higher responses, indicating poor energy coupling between the actuator and the adjacent soft tissue. Despite this, a local peak of 20.0 µm is observed at 252 Hz at the front probe. This suggests that certain higher-frequency modes can still induce localised resonances near the actuation site, even when overall response amplitudes remain low.

In the side actuator scenario (subsection 4.2.3), average displacements rise significantly beyond 118 Hz. This configuration benefits from the use of two actuators placed symmetrically, likely enabling constructive interference and more effective excitation of higher-order modes. The highest average displacement in the entire dataset, 41.4 µm at 245 Hz, occurs in this scenario. A greater number of peaks above 10 µm are also observed compared to the bottom actuator case. Local probe data (Figure 10) show broad spatial distribution of resonances. Specific frequencies, 118 Hz, 175 Hz, 204 Hz, 238 Hz, and 245 Hz activate multiple probe regions, confirming the side actuator's capability to engage both localised and global fingertip responses. Between 142–157 Hz, the bottom probe shows dominant displacements, indicating that dual side actuators can indirectly excite the underside of the fingertip as well.

Based on these results, it has become evident that the side actuator case is the most promising in producing a wide range of displacement patterns. Looking more in-depth at these patterns, Figure 11 illustrates volumetric displacement fields for selected resonance peaks in the side actuator scenario. At 118 Hz, the mode involves displacements normal to the front and side probes, suggesting possible perceptual stimuli at both sites. At 175 Hz and 204 Hz, deformations appear strongest between the front and bottom probes, likely corresponding to rotational modes affecting multiple axes. The mode at 238 Hz shows a concentration of deformation near the side and bottom probes, while the 245 Hz resonance is more complex. It combines in-phase and out-of-phase displacements across all probes, indicating that multiple high-order modes may be active simultaneously. While such combined-mode resonances may enhance vibration intensity, they could also diminish spatial specificity. For applications requiring precise spatial targeting of tactile stimuli, this may be undesirable. Conversely, when

strong global feedback is desired, these modes may be advantageous.

To improve spatial resolution and control over haptic output, reducing the number of active resonances may be beneficial. This could be achieved by either increasing the stiffness of the thimble material or decreasing its thickness. However, both changes will likely affect eigenfrequencies and displacement magnitudes, necessitating further investigation.

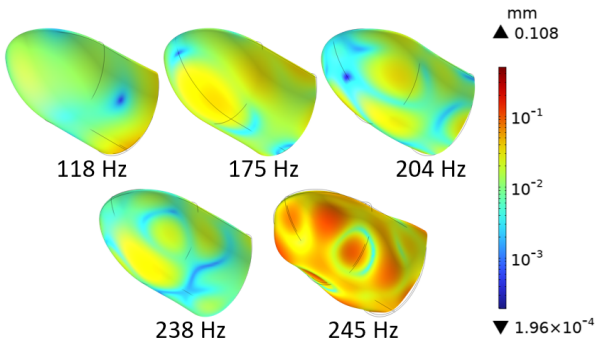

Fig. 11: The five forced vibration modes from frequencies where displacements are measured in two or more probes in the side actuation scenario. These modes are the most promising in producing different stimuli. The deformations are scaled by 10 and the colour scale is logarithmic to improve clarity.

6 Conclusion

This study presents a comprehensive finite element analysis of a haptic thimble (HapThimb) designed for the fingertip, incorporating embedded piezoelectric actuators. By extending the anatomically grounded DigiTip (Serhat & Kuchenbecker, 2024) model with a soft silicone layer and strategically placed actuators, the study examined how actuator position and excitation frequency affect vibrational behaviour and displacement distribution across the fingertip. Both free and forced vibration analyses were performed to reveal resonance phenomena, spatial deformation patterns, and implications for haptic design.

The free vibration analysis demonstrated that the addition of the thimble substantially reduces natural frequencies compared to the bare fingertip model, with the first mode decreasing from 103.53 Hz to 45 Hz. This effect was attributed to the increased mass and compliance of the thimble, in line with the classic mass–spring relationship. Moreover, the number of resonant modes in the studied frequency range increased markedly with the inclusion of the thimble, suggesting that the thimble introduces additional modal frequencies.

Forced vibration results revealed that actuator placement significantly influences both the amplitude and spatial extent of displacements. The bottom actuator produced the highest single-site displacement (53.8 µm at 185 Hz), particularly at the proximal part of the fingertip. However, it failed to stimulate other regions effectively. The front actuator, while constrained by the stiff nail plate and bed, showed a localised resonance at 252 Hz near its placement site, suggesting it may be effective in high-frequency, localised stimulation. The side actuators yielded the most versatile responses, with the greatest number of displacement peaks above 10 µm and the highest average displacement overall. Notably, the side actuator configuration activated multiple regions, including bottom, front, and side, demonstrating a broad stimulation footprint.

These findings suggest that the side actuator configuration offers the most promising design for generating diverse tactile feedback. However, highly resonant modes, such as those observed at 245 Hz, may result in global responses that reduce spatial specificity. Thus, design optimisation may require tuning thimble stiffness or geometry to balance between intensity and selectivity.

Future work should incorporate nonlinear material models, transient dynamics, and experimentally validated force-driven actuator models to better simulate real-world behaviour. Overall, the HapThimb framework offers valuable design insights for wearable haptic interfaces, highlighting the critical role of structural dynamics in shaping tactile output.

Appendix A Model Dimensions and Simulation Parameters

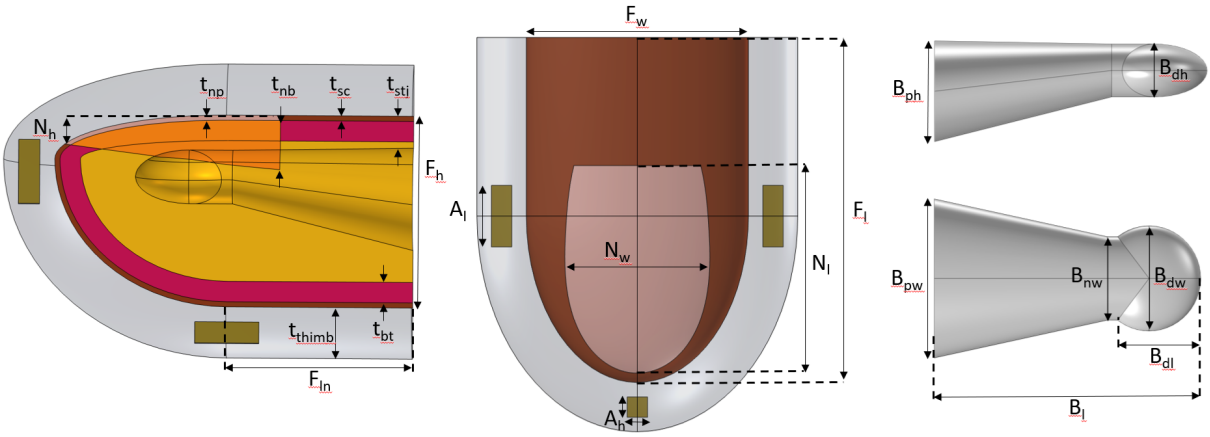

Fig. A1: The variables used in HapThimb with one exterior view, one interior view and two views of the distal phalanx.

Table A1: The descriptions and values for the model dimensions in figure A1. The values for the finger variables are from the DigiTip model (Serhat & Kuchenbecker, 2021).

Variable	Description	Value (mm)	Variable	Description	Value (mm)
F_w	Fingertip width	18	t_{stj}	Soft-tissue thickness joint	3.5
F_l	Fingertip length	28	t_{thimb}	Thimble thickness	4
F_h	Fingertip height	15	B_l	Total bone length	22.5
F_{ln}	Fingertip length to neck	14.5	B_{dw}	Bone width distal section	8.6
N_w	Nail plate width	12.3	B_{dl}	Bone length distal section	8.4
N_l	Nail plate length	17.6	B_{dh}	Bone height distal section	4.2
N_h	Nail plate height	2.5	B_{pw}	Bone width proximal section	13.0
t_{np}	Nail plate thickness	0.4	B_{ph}	Bone height proximal section	8
t_{nb}	Nail bed thickness	1.2	B_{nw}	Bone width neck	5.3
t_{sc}	Stratum corneum thickness	0.4	A_l	Actuator length	5
t_{bt}	Bulk tissue thickness	1.6	A_h	Actuator height	1.65

References

Abdouni, A., Djaghloul, M., Thieulin, C., Vargiolu, R., Pailler-Mattei, C., Zahouani, H. (2017). Biophysical properties of the human finger for touch comprehension: influences of ageing and gender. *Royal Society open science*, *4*(8), 170321,

Blanco-Diaz, C., Degl'Innocenti, G., Vendrame, E., Uliano, M., Controzzi, M., Cappello, L. (2024). Design and characterization of a low-profile haptic system for telemanipulation. *IEEE Transactions on Medical Robotics and Bionics*, ,

Brisben, A., Hsiao, S., Johnson, K. (1999). Detection of vibration transmitted through an object grasped in the hand. *Journal of neurophysiology*, *81*(4), 1548–1558,

Case, J.C., White, E.L., Kramer, R.K. (2015). Soft material characterization for robotic applications. *Soft Robotics*, *2*(2), 80–87,

Gertler, I., Serhat, G., Kuchenbecker, K.J. (2023). Generating clear vibrotactile cues with a magnet embedded in a soft finger sheath. *Soft Robotics*, *10*(3), 624–635,

Gescheider, G.A., Bolanowski, S.J., Pope, J.V., Verrillo, R.T. (2002). A four-channel analysis of the tactile sensitivity of the fingertip: frequency selectivity, spatial summation, and temporal summation. *Somatosensory & motor research*, *19*(2), 114–124,

Harris, C.M., & Piersol, A.G. (2002). *Harris' shock and vibration handbook* (Vol. 5). McGraw-Hill New York.

Huang, Y., Yao, K., Li, J., Li, D., Jia, H., Liu, Y., ... Yu, X. (2022). Recent advances in multi-mode haptic feedback technologies towards wearable interfaces. *Materials Today Physics*, *22*, 100602,

Johnson, K.O., & Hsiao, S.S. (1992). Neural mechanisms of tactual form and texture perception. *Annual review of neuroscience*, *15*, 227–250,

Johnson, K.O., Yoshioka, T., Vega-Bermudez, F. (2000). Tactile functions of mechanoreceptive afferents innervating the hand. *Journal of Clinical Neurophysiology*, *17*(6), 539–558,

Kim, M., Jeon, C., Kim, J. (2017). A study on immersion and presence of a portable hand haptic system for immersive virtual reality. *Sensors*, *17*(5), 1141,

Leroy, E., Hinchet, R., Shea, H. (2020). Multimode hydraulically amplified electrostatic actuators for wearable haptics. *Advanced Materials*, *32*(36), 2002564,

Marks, R.M., Barton, S.P., Edwards, C. (2012). *The physical nature of the skin.* Springer Science & Business Media.

Mathur, N., Mak, Y.X., Naghibi, H., Abayazid, M. (2021). A novel asymmetric pneumatic soft-surgical endoscope design with laminar jamming. *2021 43rd annual international conference of the ieee engineering in medicine & biology society (embc)* (pp. 4636–4640).

Mckittrick, J., Chen, P.-Y., Bodde, S., Yang, W., Novitskaya, E., Meyers, M. (2012). The structure, functions, and mechanical properties of keratin. *Jom*, *64*, 449–468,

Nam, S., & Kuchenbecker, K.J. (2021). Optimizing a viscoelastic finite element model to represent the dry, natural, and moist human finger pressing on glass. *IEEE Transactions on Haptics*, *14*(2), 303–309,

Pacchierotti, C., Sinclair, S., Solazzi, M., Frisoli, A., Hayward, V., Prattichizzo, D. (2017). Wearable haptic systems for the fingertip and the hand: taxonomy, review, and perspectives. *IEEE transactions on haptics*, *10*(4), 580–600,

Serhat, G., & Kuchenbecker, K.J. (2021). Free and forced vibration modes of the human fingertip. *Applied Sciences*, *11*(12), 5709,

Serhat, G., & Kuchenbecker, K.J. (2024). Fingertip dynamic response simulated across excitation points and frequencies. *Biomechanics and Modeling in Mechanobiology*, *23*(4), 1369–1376,

Shao, Y., Hayward, V., Visell, Y. (2016). Spatial patterns of cutaneous vibration during whole-hand haptic interactions. *Proceedings of the National Academy of Sciences*, *113*(15), 4188–4193,

Somer, D., Perić, D., de Souza Neto, E., Dettmer, W. (2015). A multi-scale computational assessment of channel gating assumptions within the meissner corpuscle. *Journal of Biomechanics*, *48*(1), 73–80,

Srinivasan, M.A., Whitehouse, J., LaMotte, R.H. (1990). Tactile detection of slip: surface microgeometry and peripheral neural codes. *Journal of neurophysiology*, *63*(6), 1323–1332,

Störchle, P., Müller, W., Sengeis, M., Lackner, S., Holasek, S., Fürhapter-Rieger, A. (2018). Measurement of mean subcutaneous fat thickness: eight standardised ultrasound sites compared to 216 randomly selected sites. *Scientific reports*, *8*(1), 16268,

Turner, C.H., Rho, J., Takano, Y., Tsui, T.Y., Pharr, G.M. (1999). The elastic properties of trabecular and cortical bone tissues are similar: results from two microscopic measurement techniques. *Journal of biomechanics*, *32*(4), 437–441,

Wu, J.Z., Krajnak, K., Welcome, D.E., Dong, R.G. (2009). Analysis of the biodynamic interaction between the fingertip and probe in the vibrotactile tests: the influences of the probe/fingertip contact orientation and static indentation. *Journal of biomechanics*, *42*(2), 116–124,